

## Hard Turning on JIS S45C Structural Steel: An Experimental, Modelling and Optimisation Approach

R. Kumar<sup>1\*</sup>, A. Modi<sup>1</sup>, A. Panda<sup>1</sup>, A. K. Sahoo<sup>1</sup>, A. Deep<sup>1</sup>, P. K. Behera<sup>1</sup> and R. Tiwari<sup>2</sup>

<sup>1</sup>School of Mechanical Engineering, Kalinga Institute of Industrial Technology (KIIT),  
Deemed to be University, Bhubaneswar-24,  
Odisha, 751024, India

\*Email: [ramanujkumar22@gmail.com](mailto:ramanujkumar22@gmail.com)

<sup>2</sup>Dyna Force Hydraulics Pvt. Ltd., Pune-11, Maharashtra, India

### ABSTRACT

The present research is performed while turning of JIS S45C hardened structural steel with the multilayered (TiN-TiCN-Al<sub>2</sub>O<sub>3</sub>-TiN) CVD coated carbide insert by experimental, modelling and optimisation approach. Herein, cutting speed, feed rate, and depth of cut are regarded as input process factors whereas flank wear, surface roughness, chip morphology are considered to be measured responses. Abrasion and built up-edge are the more dominant mode of tool-wear at low and moderate cutting speed while the catastrophic failure of tool-tip is identified at higher cutting speed condition. Moreover, three different Modelling approaches namely regression, BNN, and RNN are implemented to predict the response variables. A Back-propagation neural network with a 3-8-1 network architecture model is more appropriate to predict the measured output responses compared to Elman recurrent neural network and regression model. The minimum mean absolute error for VB<sub>c</sub>, R<sub>a</sub> and CRC is observed to be as 1.36% (BNN with 3-8-1 structure), 1.11% (BNN with 3-8-1 structure) and 0.251 % (RNN with 3-8-1 structure). A multi-performance Optimisation approach is performed by employing the weighted principal component analysis. The optimal parametric combination is found as the depth of cut at level 2 (0.3 mm)-feed at level 1 (0.05 mm/rev) – cutting speed at level 2 (120 m/min) considered as favourable outcomes. The predicted results were validated through a confirmatory trial providing the process efficiency. The significant improvement for S/N ratio of CQL is observed to be 9.3586 indicating that the process is well suited to predict the machining performances. In conclusion, this analysis opens an avenue in the machining of medium carbon low alloy steel to enhance the machining performance of multi-layered coated carbide tool more effectively and efficiently.

**Keywords:** JIS S45C steel; hard turning; CVD-coated cutting tool; BNN; RNN; WPCA.

### NOMENCLATURE

JIS	Japan Industrial Standard	CVD	chemical vapour deposition
AISI	American Iron and Steel Institute	ANN	artificial neural network
<i>d</i>	depth of cut (mm)	BNN	back propagation neural network
<i>f</i>	feed rate (mm/rev)	RNN	recurrent neural network
<i>v</i>	cutting speed (m/min)	BUE	built-up edge
HRC	Rockwell hardness	MLQ	minimum quantity lubrication

VB <sub>c</sub>	flank wear at nose (mm)	CNC	computer numerical control
R <sub>a</sub>	arithmetic surface roughness (µm)	RSM	response surface methodology
CRC	chip reduction coefficient	TiN	titanium nitride
ANOVA	analysis of variance	TiCN	titanium carbide nitride
HV	Vickers micro-hardness	Al <sub>2</sub> O <sub>3</sub>	aluminium oxide
R <sup>2</sup>	coefficient of determination	R <sup>2</sup>	predicted R <sup>2</sup>
		(Pred)	
R <sup>2</sup> (adj)	adjusted R <sup>2</sup>	K	number of inputs
MAE	mean absolute error	DF	degrees of freedom
SS	sum of squares	MS	mean square
P	probability of significance	F	variance ratio
CQL	combined quality loss	PCC	Pearson's correlation coefficient
WPCA	weighted principal component analysis	MPI	multiple response performance index
CAP	cumulative accountability proportion		

## INTRODUCTION

Hard part turning is regarded as an imperative manufacturing technology for increased part quality, productivity, and enhanced surface integrity. Further, this emerging process has been explored as a cost-effective substitute for the conventional finish grinding, which is used to generate components made of hardened steels. Hard part turning is a process performed on hardened materials (hardness greater than 45 HRC) to attain the level of surface roughness closer to the conventional grinding process. The technological advancement of this innovative technology is developing with the incorporation of newer advanced cutting tools for example cemented carbide, ceramics, and cubic boron nitride and polycrystalline diamond. The focal goal of the manufacturers and scientific researcher of this new process is the production of quality components and behaviour of new cutting tool material during the process [1]. Indeed, the crucial significant characteristics of hard turning are noticeable removal of material in a single operation rather than an extensive grinding process to diminish production processing time, cost of production, surface quality, and setup time to remain competitive.

The hard-turning process renders many advantages over conventional grinding. Moreover, the performance measures like cutting tool wear, tool span, surface quality, and amount of material removed are also can be predicted by this process [2]. To achieve higher productivity, more elasticity and avoidance of coolants turning of hardened steel is the appropriate machining process nowadays [3]. Also, this technique is considered as a sustainable manufacturing process due to low energy consumption [4]. Production of hardened steel parts is gaining popularity in shop floor due to its superior characteristics such as resistance to indentation, abrasiveness etc. Thus, assessment of the different machining characteristics of hardened steel is necessary to ensure that cutting operations are important manufacturing process to remain in the competitive market [5]. Hard turning process performance was majorly influenced by various factors namely workpiece hardness, cutting tool material, tool coatings, tool geometry, cutting parameters and cutting environment (Figure 1) [6]. However, various attempts have been performed to analysis the sway of these factors on measured variables during the hard-turning process.

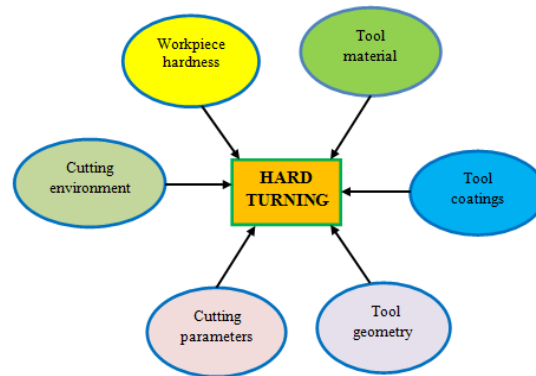


Figure 1. Major influencing terms for hard-turning.

In the hard part turning, the cutting tool gets fail due to mechanical breakage, plastic deformation, and gradual wear. Mechanical breakage and plastic deformation of the tool may be considered as a premature tool failure and can be avoided by using appropriate tool material, tool geometry and cutting conditions (cutting parameters and cutting surroundings). Gradual wear is a continuous process and it can't be prevented but it can be minimised by selecting appropriate cutting agents [7]. Chinchankar and Choudhury [7] reported various tool wear pattern like nose wear, flank wear, notch wear, crater wear, chipping, catastrophic failure and BUE in hard turning. Sampaio et al. [8] examined abrasive-tool-wear pattern under dry and MQL machining surroundings as a result, flank, as well as crater, wear was dominant. Notch marks were also seen at the end boundary of the secondary cutting edge. Singh et al. [9] explored the various tool mechanisms in turning of AISI 304 steel under three different cutting surroundings namely dry, flooded and nanofluid MQL. The mechanism like micro-chipping, abrasion, adhesive, oxidation, and severe notching are dominant under dry cutting condition. Kumar et al. [10] stated that the diffusion and abrasion wear approach was dominant in dry cutting of D2 hard steel. Diffusion mechanism is the key agent for catastrophic breakage of uncoated carbide insert.

Very limited research works have been performed on hard turning on JIS S45C steel. A brief detail overview is summarized as follows: In the machining investigation on S45C steel, the feed rate was identified as the most impactful factor towards the rate of tool wear as well as cutting tool temperature. Cutting speed was highly sensitive towards stress and growth of cutting zone temperature i.e. improvement in cutting speed attributed the higher magnitudes of stress on the tool as well as finish test specimen [11]. Machining of JIS S45C steel in dry scenario attributed the best quality of finish over wet and cryogenic cooling using CVD coated tool [12]. The higher stability of the cutting tool was noticed when machining was carried at 100 m/min but at higher speed 200 mm/min, the wear rate was increasing speedily with the progress of cutting time. Also, the cutting temperature was elevating with cutting speed [13]. The feed rate followed by nose radius contributed the highest impact on surface roughness ( $R_a$  and  $R_z$ ) in CNC turning process on S45C steel [14]. In machining on S45C steel by coated carbide TiN insert, tool-nose-chipping phenomena in the majority of tests were noticed because of elevated cutting temperature and the stress on the cutting tool-tip [15]. Erkan et al. [16] predicted artificial neural network (ANN) models by five learning algorithms for analysis of the damage factor to minimise the number of time-consuming trials. Henceforth, the highest successful performance

was attained by 4-10-1 network structure with LM learning algorithm. Especially, ANN was predicting successful in the damage factor owing to higher  $R^2$  (more than 0.999) and lower RMSE and MEP during end milling of GFRP composite material.

In recent years, various numerical methods are popularly implemented to predict the various response parameters in hard turning process due to knotty interaction between the tool-workpiece during the cutting. Yet, proper selection modelling methods is a challenging assignment for the researchers. Brief works considering the application of distinguish modelling methods in hard turning have been reported here. Mia and Dhar [17] implemented the RSM, fuzzy interface and simulated annealing to develop and co-relate the models in dry hard turning. RSM contribute to the highest determination coefficient among all. Workpiece hardness attributed the key variable on surface roughness while the combination of higher cutting speed, lower cutting feed, and lower work hardness exhibited the lower value of surface roughness. Meddour et al. [18] elaborated the influence of various cutting factors namely nose radius, cutting speed, depth of cutting and feed rate on surface roughness and forces with well-known RSM tools. The cutting speed was successfully reduced the unfavourable influence of feed on surface roughness. Labidi et al. [19] developed analytical models for surface roughness, tooling flank wear, and tangential force. The ANN approach superiorly worked for predicting the process turning parameters relative to RSM. Das et al. [20] implemented a regression analysis, analysis of variance, and main effect graphs to study the machining characteristics in turning of 4340-grade steel. Uniform growth in the wear of carbide insert was identified with a rise in cutting speed. Kumar et al. [21] implemented the regression as well as ANN to predict the tooling flank wear, surface roughness level and cutting tool temperature turning of hardened AISI D2 steel. Labidi et al. [19] applied ANN and RSM methods to predict the responses. ANN methodology attributed the better accuracy results over RSM during hard turning on X210Cr12 steel with CC6050 ceramic coated tool. Paturi et al. [22] analysed the outcomes of turning factors on surface roughness during regression and ANN models. The ANN predictions are closer to actual results and thus efficiently predict the machining responses for a proper understanding of the complex cutting phenomena. In the recent investigation, Yıldırım et al. [23] observed that the lowest wear among all type of tools is obtained under MQL machining, while the highest level of wear is obtained under wet cooling machining. Finally, MQL attributed the 17.34% and 433.67% better tool wear as compared to dry and wet cooling machining respectively.

Based on the review, many researchers have performed a comparative performance analysis of various cutting tools in hard turning. Coated carbide tools (CVD/PVD coated) are performing well in hard turning but there are lots of scopes to carry out the research taking a different combination of coating layers on to the carbide substrate. Analysis of hard turning through experimental, Modelling and optimisation together is rarely listed in the literature. Modelling in hard turning through regression and response surface methodology is majorly available in the literature. Application of ANN in hard turning modelling is inadequate and need to be explored more considering distinguish neural network parameters. Further, the recurrent neural network (RNN) modelling in hard turning is not available in the literature. Various multi-response optimisation techniques like grey relational analysis, TOPSIS, Weighted principal component analysis (WPCA), etc. are found in the literature. Responses like tool-wear, surface roughness, chip morphology are commonly available in literature but analysis of cutting-temperature and chip reduction coefficient in hard turning is rarely available. Referring to aforesaid review, it is scrutinised that multi-layered CVD (TiN-TiCN- $Al_2O_3$ -TiN) coated

carbide cutting tool with an intermediate layer of  $\text{Al}_2\text{O}_3$  requires more exploration in terms of machining characteristics to have a better understanding of its superlative performance during machining of structural steel grade. Study on the effect of main cutting parameters on intended machining output variables like surface roughness, tool wear, chip morphology, and chip reduction coefficient is inadequate during machining of JIS 45C structural steel.

Hardened JIS S45C Steel is a structural steel grade and it has numerous applications in motor shaft, shaft studs, keys and automotive parts making industries. Till date, very few amounts of experimental schemes on JIS S45C steel are listed in the literature, therefore the detailed investigation along with Optimisation and Modelling are worth needed to examine the machining performance of JIS S45C Steel. Therefore, in this context, the current investigation of JIS S45C steel having hardened condition (52-55 HRC) is selected to study the various parametric influences on multi-responses using multi-layered coated carbide insert under dry condition. Further, three different Modelling techniques (Regression, Artificial neural network (ANN) and recurrent neural network (RNN)) are implemented to predict the multi-responses and their results are compared. RNN is a neural base Modelling technique and not used yet for hard turning applications. Further, to achieve the appropriate optimal settings of cutting factors, WPCA coupled with Taguchi approach has been implemented for the multi-response optimisation.

## MATERIALS AND METHOD

The work-specimen JIS S45C steel with hardness range of 52-55 HRC is selected for this experimental study. The finishing length and initial diameter of the workpiece are 90 mm and 36 mm respectively. The chemical constituents of work-specimen are presented in Table 1. The multi-layered CVD ( $\text{TiN-TiCN-Al}_2\text{O}_3\text{-TiN}$ ) coated carbide cutting tool of geometry CNMG 1204085 (TN 7105) and made by WIDIA, Germany has been implemented for hard turning process. The Vickers microhardness of insert has been measured three times at a load of 1 kg ( $\text{HV}_1$ ) with diamond indenter and indenter shape is displayed in Figure 2. The average microhardness is found as 1865  $\text{HV}_1$  and it shows a higher grade of wear-resistance capability of the insert. The tool holder of ISO configuration PCLNR2525M12 is used to screw the rhombus-shaped insert with a nose radius of 0.85 mm. CNC centre lathe (spindle speed = 50 to 4000 rpm) made by Jyoti CNC Automation Ltd. is utilised for the experimentation.

Table 1. Constituents of JIS S45C hardened steel.

Constituents	C	Mn	Si	Ni	Cr	Mo	S	P
wt.%	0.49	0.74	0.20	0.108	0.11	0.017	0.005	0.014

Taguchi $L_{16}$  experimental design has been chosen based on three input cutting terms (cutting speed,  $v$ ; feed,  $f$ ; and depth of cut,  $d$ ) and four levels as in Table 2. The responses to be measured are flank wear ( $\text{VB}_c$ ), average surface roughness ( $R_a$ ) and chip-reduction coefficient (CRC). The standard limit of  $\text{VB}_c$  and  $R_a$  have been fixed as 0.3 mm and 1.6 microns respectively [20, 24-26]. Width of flank wear is measured through optical micrographs images which are captured offline via STM6 microscope whereas Taylor Hobson's roughness tester is utilised for  $R_a$  measurement and followed the ISO 3274-1996 standard. The roughness tester set up parameters like the number of sampling, cut off length and assessment length are 5, 8 mm

and 4 mm respectively used during surface roughness measurement. Five different locations on the turned surface in the axial direction are chosen to measure the  $R_a$  and the average data is noted for the study. After completion of each experiment, chip samples are collected and randomly thickness of five samples is measured and the average thickness is taken. MINITAB-16 statics tool is used for ANOVA and main effects plot. Matlab R2013a software is utilised to carry out the ANN and RNN Modelling. The graphical view of the entire work has been reported in Figure 3.

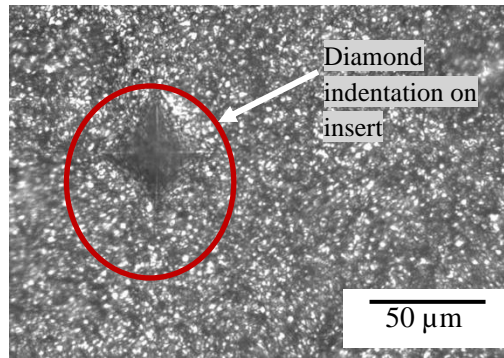


Figure 2. Indentation marks on cutting insert.

Table 2. List of parameters and their levels.

Factors	Levels			
	1 <sup>st</sup>	2 <sup>nd</sup>	3 <sup>rd</sup>	4 <sup>th</sup>
$v$ (m/min)	60	120	180	240
$f$ (mm/rev)	0.05	0.15	0.25	0.35
$d$ (mm)	0.2	0.3	0.4	0.5

Table 3. Experimental evaluation.

Run	$d$ (mm)	$f$ (mm/rev)	$v$ (m/min)	$VB_c$ (mm)	$R_a$ ( $\mu$ m)	CRC	Chip Shape	Chip Colour
1	0.2	0.05	60	0.077	0.552	1.867	Helical	Metallic
2	0.2	0.15	120	0.093	0.644	1.673	Ribbon	Metallic
3	0.2	0.25	180	0.112	0.912	1.445	Ribbon	Metallic
4	0.2	0.35	240	0.143	1.544	1.337	Ribbon	Metallic
5	0.3	0.05	120	0.089	0.438	1.766	Helical	Metallic
6	0.3	0.15	60	0.101	0.902	1.806	Ribbon	Metallic
7	0.3	0.25	240	1.121	1.168	1.485	Ribbon	Metallic
8	0.3	0.35	180	0.176	1.887	1.405	Ribbon	Metallic
9	0.4	0.05	180	0.117	0.668	1.827	Helical	Metallic
10	0.4	0.15	240	0.988	1.064	1.74	Ribbon	Metallic
11	0.4	0.25	60	0.115	1.422	1.806	Ribbon	Metallic
12	0.4	0.35	120	0.149	1.98	1.577	Ribbon	Metallic
13	0.5	0.05	240	0.168	0.801	1.927	Helical	Metallic
14	0.5	0.15	180	0.135	0.845	1.847	Ribbon	Metallic
15	0.5	0.25	120	0.125	1.182	1.887	Broken	Metallic
16	0.5	0.35	60	0.114	2.008	2.007	Broken	Metallic

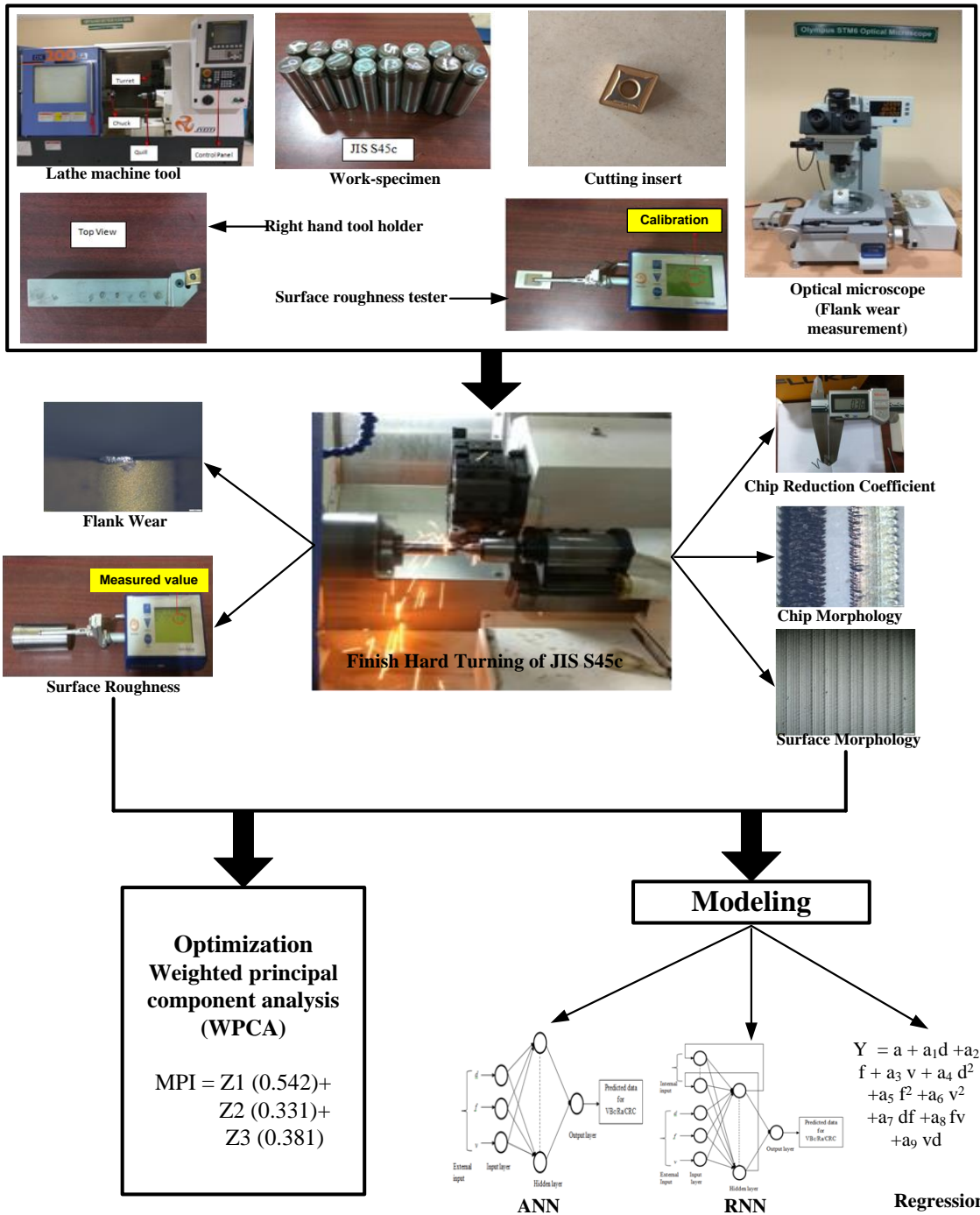


Figure 3. Graphical view of entire work.

## RESULTS AND DISCUSSION

### Wear Morphology

For hard turning concern, failure of the cutting tool in various mode of wear is found as a prime issue which leads to a tooling cost. However, it needs to be elaborated precisely to understand the role of various factors towards tool wear and also how these factors can be controlled for minimisation of tool wear thus tooling cost. In the current research work, flank wear is measured after the completion of each experiment and displayed in Table 3. The wear data depicts the favourable machining as wear width lies within the recommended limit of 0.3 mm except for 10<sup>th</sup> and 13<sup>th</sup> run. Even machining at 180 m/min with total feed rate and depth of cutting attributes below than 0.2 mm wear width, which ensures the better capability of the multi-layered coated tool. Throughout all experiments, abrasion mode of wear mechanism is traced to be dominant due to hard constituents like chromium and silicon are present in JIS S45C grade steel. Also, rubbing between flank surface and chips promotes abrasive marks near tool-tip as shown in Figure 4. The appearance of built-up edge (BUE) is clearly perceived on to the tool nose at smallest and moderate cutting speed (60 and 120 m/min) conditions as shown in Figure 4. Catastrophic delamination of tool nose is identified at higher cutting speed with moderate feed rate and depth of cut, due to the high intensity of cutting temperature generation. Kumar et al. [27] found the catastrophic failure of TiN coated tool at 182 m/min of machining of D2 steel under dry condition. Dominancy of cutting speed on wear is clearly identified through test results [25-27].

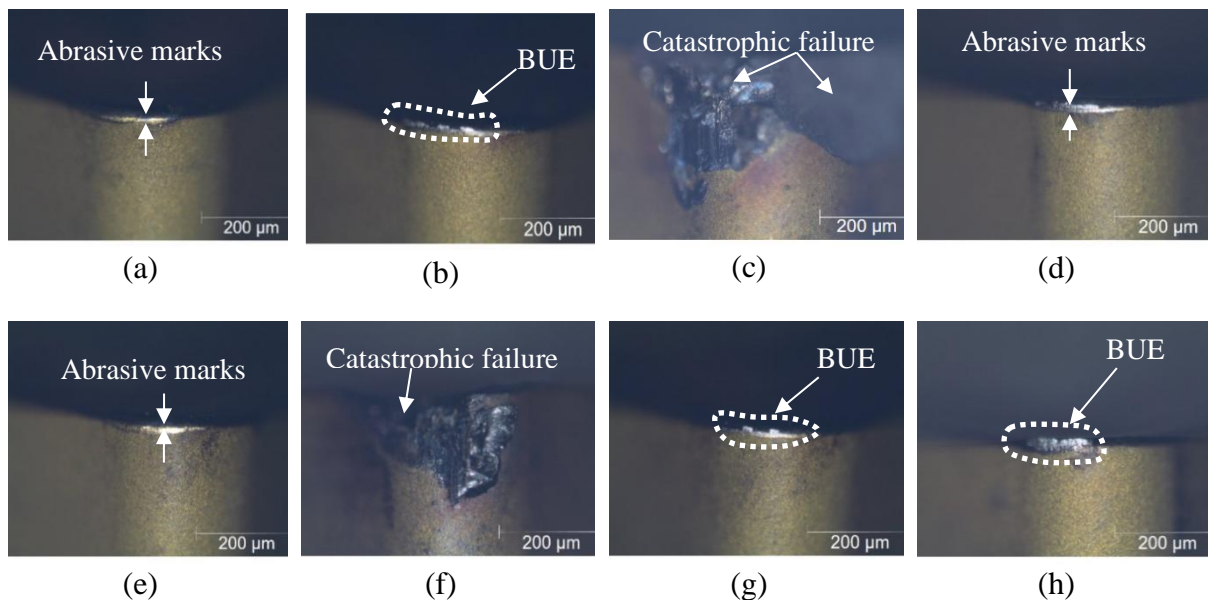


Figure 4. Flank wear images of different run.

### Surface Roughness Analysis

Surface roughness represents the waviness of a surface at the microscopic level and it is the major component for the machinability concern [28]. However, the present study emphasised

on the offline evaluation of  $R_a$  by portable surface roughness tester. Distinguish factors like cutting speed, depth of cut, feed, flank wear etc. directly or indirectly affects the surface quality of the freshly machined component. Therefore, the consequences of these parameters on surface roughness are discussed.

From Table 3, it has been clearly noticed that in most of the cases (except the 8<sup>th</sup> and 16<sup>th</sup> run) the surface roughness lies below the standard roughness criteria of  $1.6 \mu\text{m}$  [20, 24-25]. The roughness values are observed to be beyond to  $1.6 \mu\text{m}$  for highest feed  $0.35 \text{ mm/rev}$  condition. Hence for surface roughness concern, the tool performed well up to  $0.25 \text{ mm/rev}$  with entire ranges of considered cutting speed and depth of cut. For surface roughness concern, the cutting speed doesn't contribute a significant change while a minor improvement in  $R_a$  is noticed when the depth of cut rises to  $0.4 \text{ mm}$  beyond it marginally decreases. Initially (up to run 7),  $R_a$  is increasing with leading wear width whereas in other conditions, the effect of feeds on  $R_a$  is more dominant than wear width.

The surface topology of the machined surface clearly correlates the feed with feed marks. The gap between two consecutive feed marks increases with feed rate i.e. higher feed attributes wider feed marks and vice versa. The surface topology at run 1 ( $0.05 \text{ mm/rev}$ ) and run 4 ( $0.35 \text{ mm/rev}$ ) are displayed in Figure 5, which clearly shows the effects of feed on the gap between two consecutive feed marks i.e. higher feed produces wider feed marks and vice versa condition. At the higher cutting speed ( $240 \text{ m/min}$ ) and feed ( $0.35 \text{ mm/rev}$ ) condition, some fine pieces of chips are adhered on the finished surface due to high-temperature generation. Similar observations were reported by Kumar et al. [29].

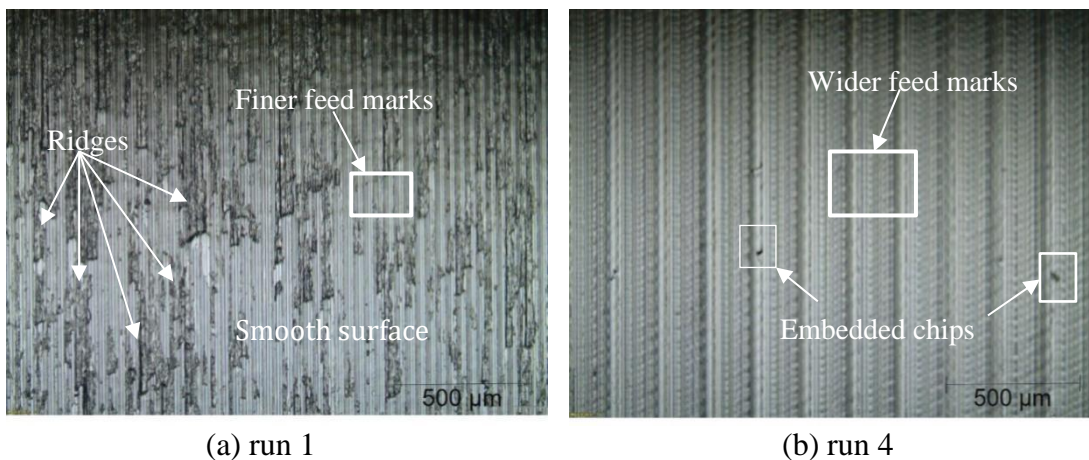


Figure 5. Surface topology of the finished surface using optical microscope.

### Chip Morphology and Chip Reduction Coefficient

The shape and colour of chips for each run is listed in Table 3. In most runs, the shape of chips is observed as ribbon type. Ribbon type of chips is bonded types of a structure where chips are bonded together and form a long and continuous strip. The bottom portion of chips has steps marks due to intermittent slip while the outside portion is smooth and shining as shown in (Figure 6(a)). Snarl type helical chips (Figure 6(b)) are generated at the lowest feed  $0.05 \text{ mm/rev}$  condition and indicates favourable machining as the smoother surface is produced. Broken

discontinuous types chips in Figure 6(c) were produced at more feed and highest depth of cut condition which attributes the relatively rough surface and not favourable for hard turning concern [10]. In the entire set of experiments, the colours of chips are metallic which indicates the optimum amount of heat generation during the process. In each run, sawtooth profile (as shown in Figure 6) on the chip is noticed due shear cyclic crack formation on to the thin sections of the chips [10, 26]. According to Ueda et al. [30], sawtooth is formed due to high stain concentration by local weakening through high heat penetration into the workpiece.

Chip reduction coefficient (CRC) introduced the frictional characteristics of any conventional machining process. Higher CRC denoted the higher frictional coefficients which attributed the higher cutting force thus higher specific power requirements for cutting the metal. The lower value of the chip reduction coefficient signifies lesser vibrations and chattering with efficient chip production [25, 31]. However, higher CRC represents poor machinability performance. In the current work, higher CRC is noticed at a higher depth of cut (0.5 mm) conditions (Table 3). Also, CRC is higher at smaller feed conditions (0.05 and 0.15 mm/rev condition). These observations clearly indicate the higher cutting force as well as higher specific cutting power requirement to cut the materials compared to other machining conditions.

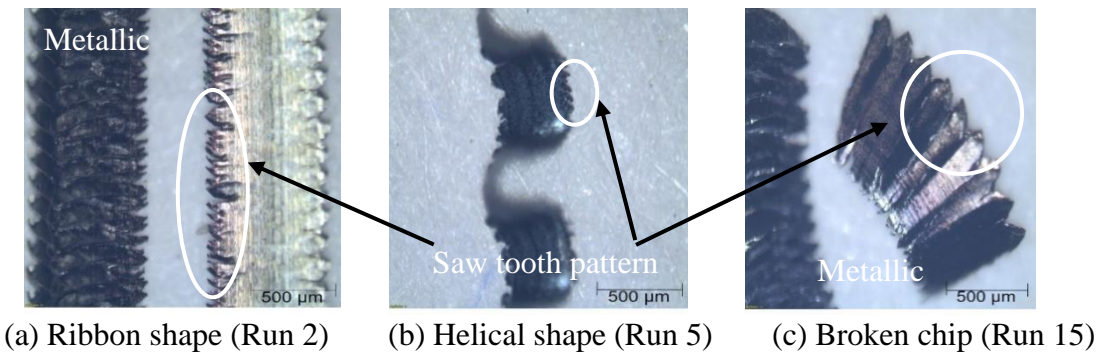


Figure 6. Different types of chips pattern.

### Parametric Effects Study through Graphical Plots and ANOVA

Graphical view clearly shows the variation in responses with respect to levels of cutting factors. Currently, the main effects plot and interaction plots are studied and the same are discussed subsequently. From the main effects plot in Figure 7(a),  $VB_c$  is clearly improving with cutting speed but the rate of wear is very slow till 180 m/min of machining, beyond it the  $VB_c$  is rapidly increasing due to poor stability of insert at highest speed and it is validated from the experimental results (run 7 and run 10). The sway of the depth of cut and feed are marginal as the graph is distributed near to the mean line. Likewise, from Figure 7(b), cutting feed is seemed to be the most dominating factor as roughness increasing almost linearly with improving cutting feed. As the graph of  $R_a$  for cutting speed and depth of cut is varied along mean line, hence it can be said that the effects of these parameters are insignificant. In a similar way from Figure 7(c), all three parameters ( $d$ ,  $f$ , and  $v$ ) affected the CRC significantly and among these three parameters influence of depth of cut is the largest [10].

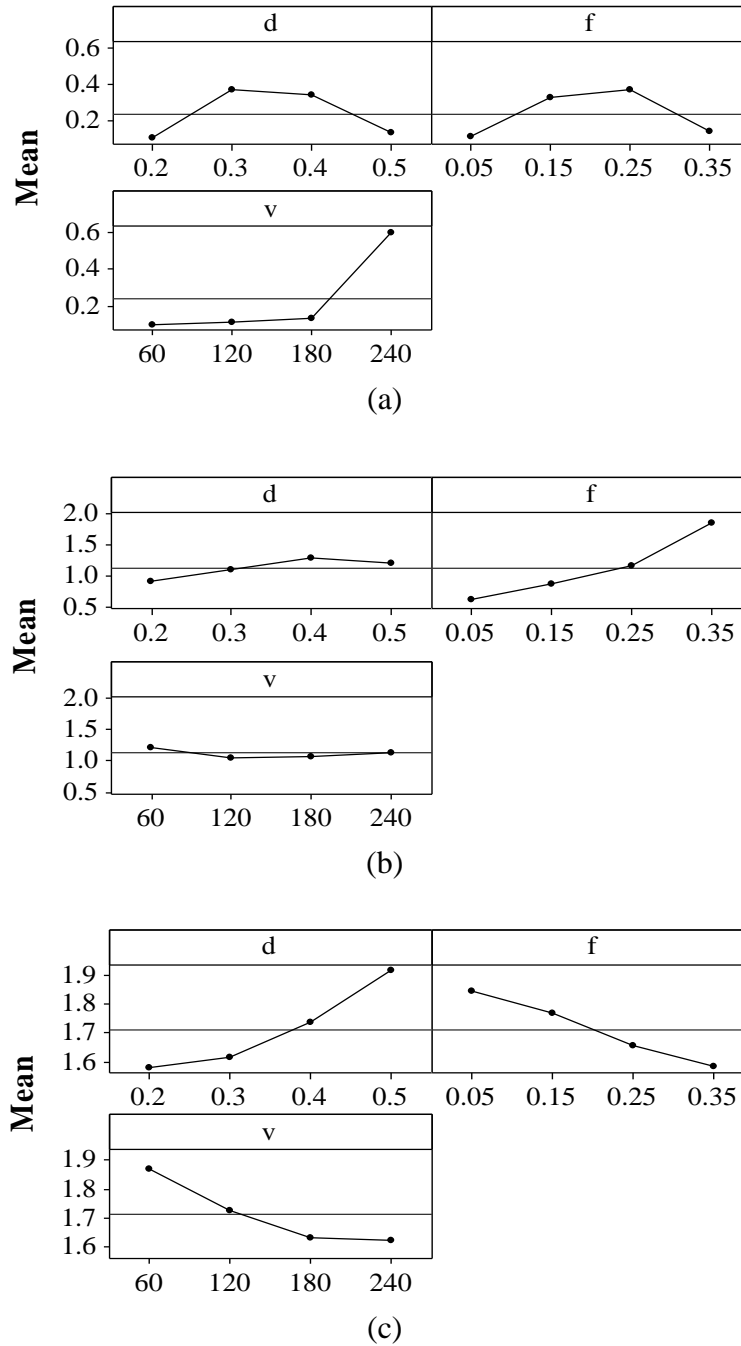
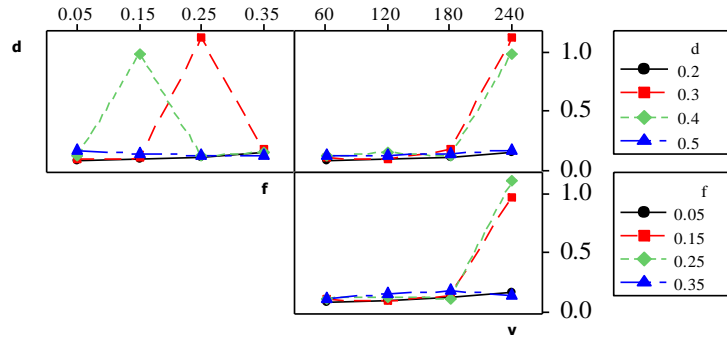


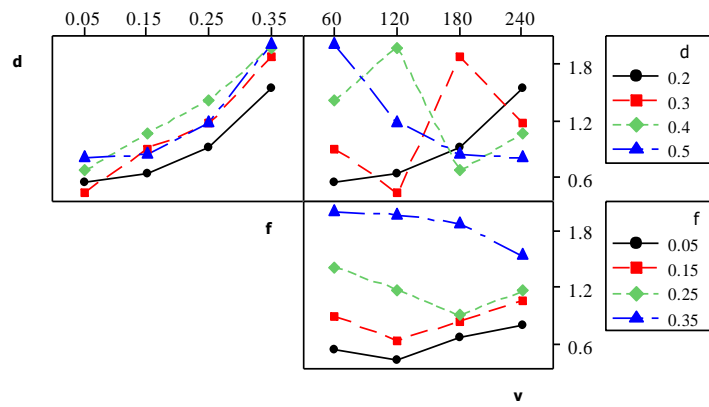
Figure 7. Main effects plots for (a) VB<sub>c</sub> (b) R<sub>a</sub> (c) CRC.

Interaction plot deals the interaction effects through graphical illustration and attributing the better realization of interactions between the control parameters that are selected. Interaction between the factors exists, when the graph lines are non-parallel and not exist for the parallel graph lines [32]. Interaction plots for all responses (VB<sub>c</sub>, R<sub>a</sub>, and CRC) are displayed in Figure 8(a), 8(b) and 8(c) respectively. For response VB<sub>c</sub>, the interaction effect doesn't exist for any

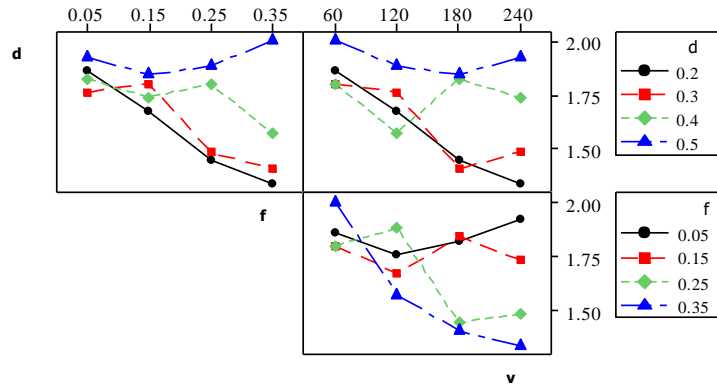
combinations as lines are parallel. Similarly, for response  $R_a$ , a strong interaction exists for  $v$ - $f$  and  $v$ - $d$ . For CRC, the interaction effect of all the couple terms like  $v$ - $f$ ,  $v$ - $d$ , and  $f$ - $d$  exist.



(a)



(b)



(c)

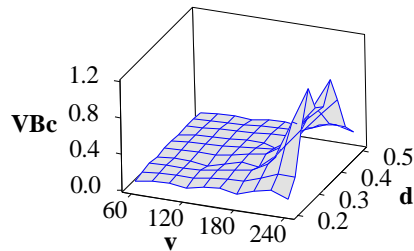
Figure 8. Interaction plots for (a)  $VB_c$  (b)  $R_a$  (c) CRC.

From the surface plot of  $VB_c$  in Figure 9, the surface is lifting upwards after 140 m/min of speed this ensure that the flank wear rapidly increases when cutting speed exceeds to 140

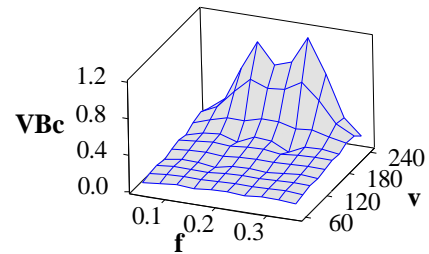
m/min and it is evident from ANOVA which shows the contribution of speed towards  $VB_c$  is 46.54%. Effects of the depth of cut and feed are not exactly identified due to uneven variations in surface and it confirms through ANOVA contribution value where the contribution of the depth of cut and feed is 14.7% and 12.86%. Similarly, from the surface plot of  $R_a$ , the surface slope is increasing with feed rate whereas the consequences of the depth of cut and cutting speed are marginal. Hence, it can be stated that the surface roughness is highly dominated by feed and it is confirmed by ANOVA (Table 4) where the contribution of feed towards  $R_a$  is 88.92%. Similar way, the surface slope of CRC is leading with depth of cut and minimising with feed and cutting speed which shows that the CRC is affected by all three cutting terms ( $v$ ,  $f$ , and  $d$ ) and among them, depth of cut is highly dominant which is confirmed from ANOVA which ensures the highest contribution of depth of cut (44.83%) towards CRC. Similar observations were reported by Kumar et al. [25, 27].

Table 4. Estimation of contribution of factors using ANOVA.

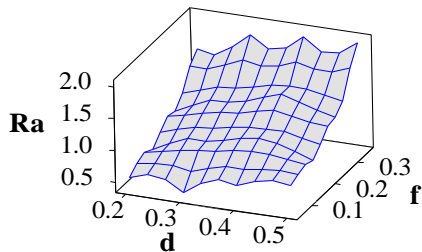
Factors	Turning outputs		
	$VB_c$ (%)	$R_a$ (%)	CRC (%)
$v$ (m/min)	46.54	01.63	26.04
$f$ (mm/rev)	12.86	88.92	26.73
$d$ (mm)	14.70	08.01	44.83
Error	25.90	1.44	2.4
Total	100	100	100



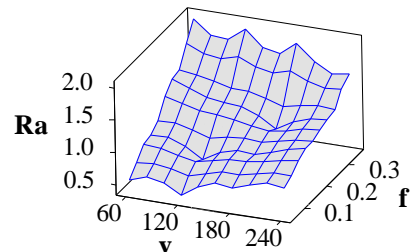
(a) flank wear



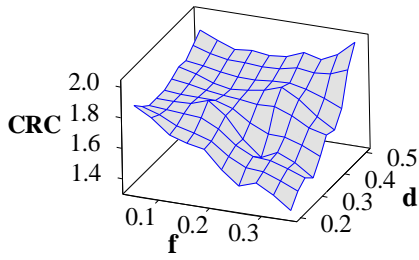
(b) flank wear



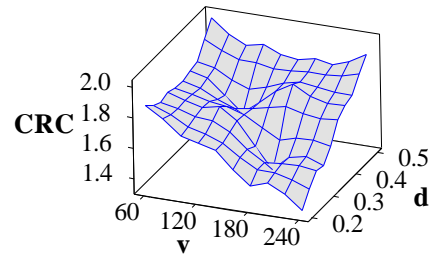
(c) surface roughness



(d) surface roughness



(e) chip reduction coefficient



(f) chip reduction coefficient

Figure 9. 3D surface plots.

## Empirical Modelling

### Regression modelling

The second-order regression models establish a functional bonding between input variables ( $v$ ,  $f$ , and  $d$ ) and a particular response ( $Y$ ) as shown in the Eq. (1).

$$Y = a + a_1d + a_2f + a_3v + a_4d^2 + a_5f^2 + a_6v^2 + a_7df + a_8fv + a_9vd \quad (1)$$

In Eq. (1), ‘ $Y$ ’ symbolizes as the output response, ‘ $a$ ’ is the intercept of the plane and ‘ $a_1$ ’, ‘ $a_2$ ’, ..... ‘ $a_9$ ’ symbolise as the regression coefficients which depend on the main effects and calculated using least square theories. The terms ‘ $d$ ’, ‘ $f$ ’ and ‘ $v$ ’ are the input parameters and  $d^2$ ,  $f^2$ , and  $v^2$  are the square terms while ‘ $df$ ’, ‘ $fv$ ’, and ‘ $vd$ ’ are interaction terms [25, 33].

In the current investigation, three regression models namely  $VB_c$ ,  $R_a$  and CRC are established and showing high degrees of  $R^2$  (about 100 %),  $R^2(\text{predicted})$  and  $R^2(\text{adjacent})$  at 95% of confidence. Therefore, these models are statistically significant and able to predict the responses.

$$VB_c = -0.1017 + 3.7256d - 3.2613f - 0.0043v - 11.8062d^2 - 10.9812f^2 + 22.1489df + 0.0014dv + 0.0008fv \quad (2)$$

$$R^2 = 99.41\% \quad R^2(\text{pred}) = 94.34\% \quad R^2(\text{adj}) = 98.52\%$$

$$R_a = 0.3751 + 3.1523d + 1.0797f - 0.0082v - 6.5062d^2 + 10.8687f^2 + 0.8170df + 0.0131dv - 0.0065fv \quad (3)$$

$$R^2 = 99.39\% \quad R^2(\text{pred}) = 93.03\% \quad R^2(\text{adj}) = 98.46\%$$

$$CRC = 2.2767 - 1.6833d - 1.6889f - 0.0025v + 3.6125d^2 + 0.1500f^2 + 2.6931df - 0.0254dv - 0.0023fv \quad (4)$$

$$R^2 = 99.05\% \quad R^2(\text{pred}) = 92.28\% \quad R^2(\text{adj}) = 97.62\%$$

## Neural Network Modelling

Current work elaborates the ANN Modelling to predict the hard-turning response variables ( $VB_c$ ,  $R_a$ , CRC). ANN worked on the biological concept of the human brain and its nervous systems. Most popular Back-propagation algorithm is utilised to process the ANN Modelling. ANN comprises of input, hidden and output layers. Input layer comprises of various neurons (distinguish inputs) which are connected to individually to each neuron of the hidden layer. Similarly, the hidden layer also consists of various neurons which are further connected to each neurone of the output layer. The output layer consists of single or multi-neurons (depends on users) and provides the predicted output response data [34-35].

### *Back-propagation neural network*

Back-propagation neural network (BNN) composed of three various layers, namely input, intermediate or hidden and output layers as shown in Figure 10. In training of the network, the calculations are computed from input to the output layer, and error data are then transmitted back to the consequent layer. Three individual inputs ( $K=3$ ), specifically cutting speed ( $v$ ), feed rate ( $f$ ) and depth of cut ( $d$ ) are taken together with an individual response (flank wear:  $VB_c$  / surface roughness:  $R_a$  / chip-reduction coefficient: CRC). In between the input and output layer, a hidden layer is placed. Three different architectures of the hidden layer, namely  $2K$  (6 neurons),  $2K+1$  (7 neurons),  $2K+2$  (8 neurons) are chosen based on previous research work. Zhang et al. [31] purposed that the number of neurons in the hidden layer can be based on the number of inputs 'K' and the number of neurons in the hidden layer may vary as  $K$ ,  $K/2$ ,  $2K$ ,  $2K + 1$  number of neurons. Also, according to Panchal et al. [36], by keeping more number of neurons in the hidden layer, the more accurate result is achieved. However, in this work, three different numbers of neurons in hidden layers are chosen. Levenberg-Marquardt (L-M) algorithm is utilised for training of the network. Mean square error in prediction is taken as a performance standard for the network.

## Recurrent Neural Network (RNN) Modelling

RNN is different from back-propagation NN Modelling. RNN is a neural network by a feedback loop and figures a closed-loop for the network. RNN is a combining form of feedforward and back forward structure [37-38]. Generally, Elman Network and Jordan Network are most popular RNN algorithms and the learning process of these networks chases the gradient descent technique [30].

### *Elman network*

Elman network is a three-layer feed-forward back propagation neural network by an additional context layer (input layer of Elman network is consist of together internal and external neurons). In addition, the external inputs are appropriately fed into the Elman network and feedbacks are received from hidden neurons [39]. The net outputs of the hidden neurons are fed back as internal inputs to the developed network as shown in Figure 11. In general, the connecting weights among hidden and context neurons are reserved to be fixed. Connecting weights for input-hidden layer and hidden output layers are updated during the training while, feedback

connection weights are remained fixed. The diagram architecture of the Elman recurrent neural network is displayed in Figure 11. Similar to BNN, Levenberg-Marquardt (L-M) algorithm is utilised for the training of the network and mean square error is considered as a performance criterion for the network. Similar to BPNN, three different hidden layer 2K (6 neurons), 2K+1 (7 neurons), 2K+2 (8 neurons) are used for the RNN modelling [35].

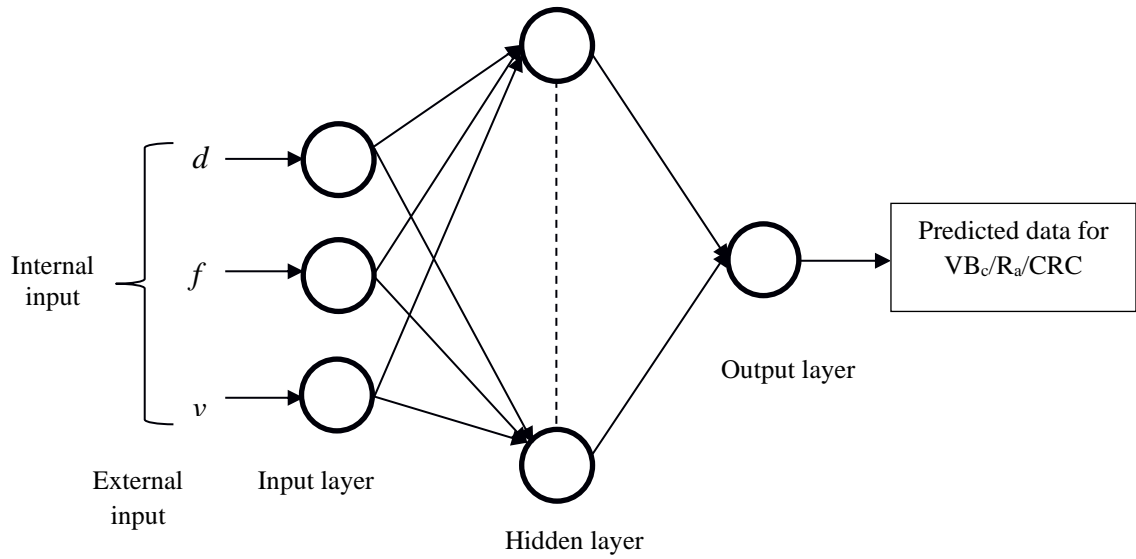


Figure 10. Architecture of back-propagation neural network.

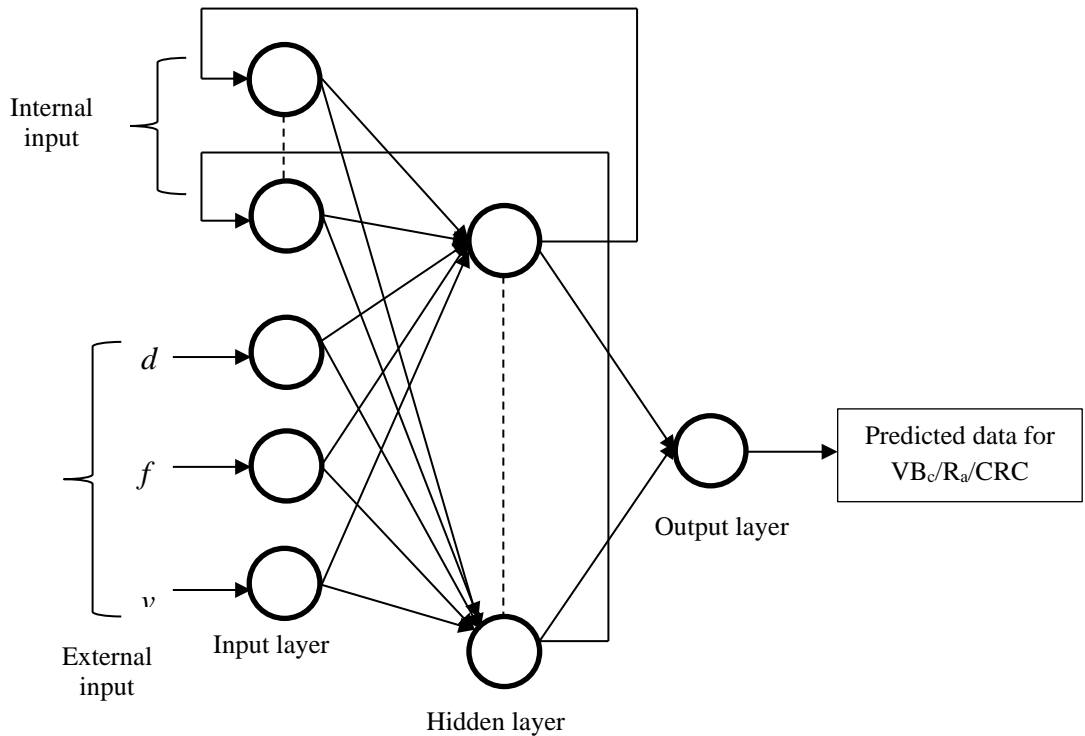


Figure 11. Architecture of recurrent neural network

### Procedure to Carry Out ANN and RNN Modelling

Matlab R2013a is used to accomplish the ANN and RNN modelling. In Matlab, ‘nntool’ is utilised to adopt feed-forward back-propagation network and Elman network. The different NN functions like ‘dividerand’ for random data distribution, ‘trainlm’ for training the input data, ‘leargdm’ for learning, ‘mse’ for examining the performance, ‘tansig’ for transferring the data have been taken. By default, the activation function “Tan-Sigmoid” was used in both modelling. To train both networks, training parameters namely maximum number of epochs = 1000, initial training rate = 0.001, learning rate = 0.01, ratio to increase and decrease learning rate = 1.05 and 0.7 respectively, momentum constant = 0.9, and minimum performance gradient  $1e-7$  is used. Similar variables have been used by D’Mello et al. [40] and Kumar et al. [41]. Several trials have been performed to get desirable solutions using different initial random weights. Graphical representation of training, testing, and validation for BNN model (3-8-1) is shown in Figure 12, and it confirms the well fit of model as R2 value (All:  $R= 0.9999$ ) is close to unity. Further, the network is simulating in order to obtain the predicted value of a particular response.

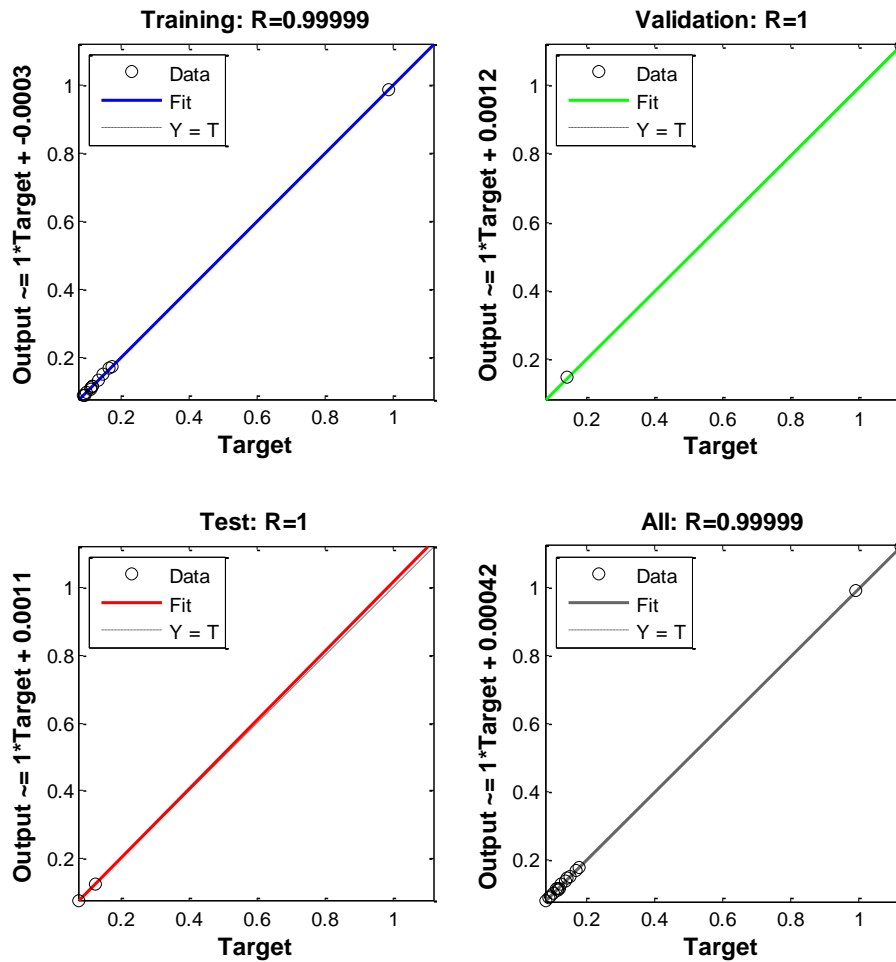
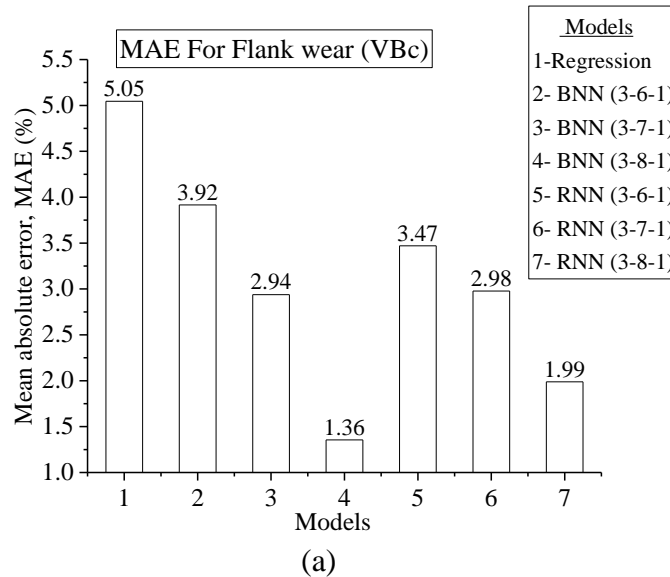


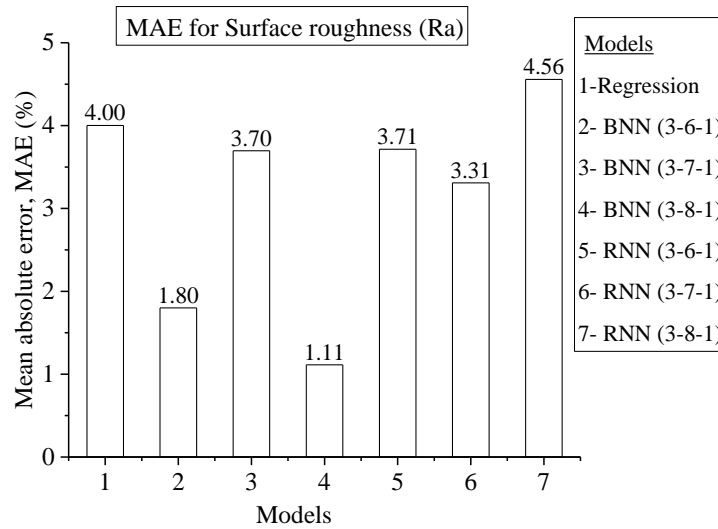
Figure 12. Graphical representation of training, testing, and validation for BNN model (3-8-1).

The prediction of L<sub>16</sub> experimental results for each response was estimated using regression, BNN (three different architectures: 3-6-1; 3-7-1 and 3-8-1) and RNN (three different architectures: 3-6-1; 3-7-1 and 3-8-1) techniques. The predicted data for each response is compared with experimental data and mean absolute error in percentage is calculated using the following relations [41-42]:

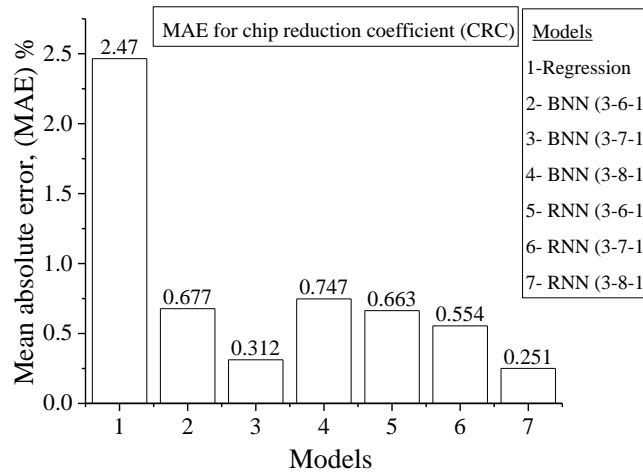
$$MAE(\%) = \sum_{i=1}^n \left| \left( \frac{E_i - P_i}{E_i} \right) \right| 100 \quad (5)$$

The mean absolute error of responses VB<sub>c</sub>, R<sub>a</sub> and CRC is graphically presented in Figure 13. For response VB<sub>c</sub> in Figure 13(a), the minimum absolute error is 1.36% which is found when BNN modelling is carried with the 3-8-1 architecture of the network. Similarly, for response R<sub>a</sub> in Figure 13(b), least error 1.11% is found with 3-8-1 network architecture of BNN modelling. Further, the minimum error of CRC in Figure 13(c) is found as 0.251% which has noticed with 3-8-1 network architecture of RNN modelling. Overall, all the modelling techniques attributed the close prediction of results as maximum MAE for VB<sub>c</sub>, R<sub>a</sub> and CRC are found as 5.05% (regression modelling), 4.56% (RNN with 3-8-1 structure) and 2.47% (regression). From this analysis, BNN with 3-8-1 network architecture attributed the best fit result for response VB<sub>c</sub> and R<sub>a</sub>. Moreover, at the same architecture, the MAE for CRC is 0.707% which is very less. However, it can be said that the BNN with 3-8-1 network architecture model is more suitable to predict the response parameters compared to other models.





(b)



(c)

Figure 13. Mean absolute error of (a)  $VB_c$  (b)  $R_a$  and (c) CRC for different models.

### Multi Response Optimisation

In this investigation, all the measured output responses are considered to have their individual effect on the part surface quality and economy in the metal cutting process. Consequently, it is necessary to optimise the measured output parameters concurrently to sustain a better balance among the part quality and cost-effective of machining. Because conventional Taguchi approach is not adequate enough to answer the multi-response optimisation troubles, thus WPCA coupled with Taguchi approach has been employed in the current study [43-44].

Weighted principal component analysis (WPCA) together with the Taguchi approach has been utilised for multi-response parametric optimisation which is must be needed for continuous quality enhancement [45]. The experimental data of multi-responses  $VB_c$ ,  $R_a$ , and

CRC are normalised taking into account ‘lower-the-better criteria’ i.e.  $K_i^*(x) = [\min K_i(x)/K_i(x)]$  where,  $K_i^*(x)$  is the normalised result of the  $x^{th}$  constituent in the  $i^{th}$  sequence and shown in Table 5. Further, Pearson’s correlation coefficient (PCC) among the response parameters has been estimated to check the correlation between responses. From Table 6, it can be stated that the PCC contains non-zero data that specifies that the outputs are correlated. Further, eigenvector and eigenvalues, accountability proportion (AP) and cumulative accountability proportion (CAP) are estimated to eliminating the response correlation and their values are shown in Table 8. MINITAB has been used to find out principal component analysis (PCA). Accountability Proportion (AP) of individual principal components is presumed as individual priority weights. Individual principal component (PC<sub>1</sub>, PC<sub>2</sub>, PC<sub>3</sub>) are known as uncorrelated quality indices which are formulated by converting into the correlated responses and presented in Table 7.

Table 5. Normalised trial data.

Sl.No	Normalised data		
	VB <sub>c</sub>	R <sub>a</sub>	CRC
Ideal	1	1	1
1	1.0000	0.7935	0.7161
2	0.8280	0.6801	0.7992
3	0.6875	0.4803	0.9253
4	0.5385	0.2837	1.0000
5	0.8652	1.0000	0.7571
6	0.7624	0.4856	0.7403
7	0.0687	0.3750	0.9003
8	0.4375	0.2321	0.9516
9	0.6581	0.6557	0.7318
10	0.0779	0.4117	0.7684
11	0.6696	0.3080	0.7403
12	0.5168	0.2212	0.8478
13	0.4583	0.5468	0.6938
14	0.5704	0.5183	0.7239
15	0.6160	0.3706	0.7085
16	0.6754	0.2181	0.6662

Table 6. Correlation check

Sl.No	Correlation between response outputs	Pearson correlation coefficient	Comment
1	VB <sub>c</sub> and R <sub>a</sub>	0.528	Both responses are correlated
2	VB <sub>c</sub> and CRC	-0.328	Both responses are correlated
3	R <sub>a</sub> and CRC	-0.338	Both responses are correlated

Table 7. PCA results.

	PC <sub>1</sub>	PC <sub>2</sub>	PC <sub>3</sub>
Eigen value	1.626	0.9923	0.3817
Eigen vector	0.704	0.038	-0.709
	0.696	0.155	-0.701
	-0.137	-0.987	-0.083
AP (Accountability proportion)	0.542	0.331	0.127
CAP (Cumulative accountability proportion)	0.542	0.873	1.000

Multiple response performance index (MPI) is overall quality index and it is computed by using the Eq. (6).

$$MPI = Z1 \times 0.542 + Z2 \times 0.331 + Z3 \times 0.381 \tag{6}$$

Further, a combined quality loss (CQL) was calculated by smaller the better' criteria and works as a single response. Further to get an optimum set of parameters, S/N ratio of CQL is estimated considering the 'higher the better' criteria. The estimated MPI, CQL and S/N ratio of CQL is listed in Table 8.

Further, the average S/N ratio of CQL is estimated and listed in Table 9. Form Table 9, the higher mean value of individual cutting parameter shows its optimum level and the optimal setting is found as *d2-f1-v2* as shown in Table 9. Further delta (maximum-minimum) value for each cutting parameter is calculated and found that the influence of feed on S/N ratio of CQL is highest as delta value (9.035) is highest for feed next cutting speed (5.324) and depth of cut (4.116). These statics are also verified through ANOVA percentage contribution (Table 10), where it is found that the contribution of feed towards S/N ratio of CQL is highest (51.77%) followed by cutting speed (16.43%) and depth of cut (16.34%).

**Confirmation Results**

The obtained optimal setting of parameters is further used for confirmation experimental test and the obtained data are listed in Table 11. Further, the predicted result is estimated at an optimal set of parameters using Eq. (7). The initial S/N ratio of CQL is taken for experimental run 1 and it is compared with results obtained at the optimum run. From this comparative analysis, the gain in S/N ratio of CQL is found as 9.3586 which about 68.3% higher than the initial setting. However, it can be concluded that the WPCA is effectively and efficiently optimise the multi-responses.

$$\gamma_p = \gamma_m + \sum_{i=1}^n (\gamma_o - \gamma_m) \tag{7}$$

where  $\gamma_p$  denotes the predicted value,  $\gamma_m$  represents the average value of GRG,  $\gamma_o$  represents the mean of GRG for individual input factor, 'i' represent the number of input term (1..... n).

Table 8. Calculation of principal components, MPI, CQL and S/N ratio.

Sl.No.	Distinct principal components			MPI	CQL	S/N Ratio of CQL
	Z1	Z2	Z3			
Ideal	1.2630	1.1800	-0.0910	1.0404	0.0000	----
1	1.1582	0.8678	-0.2122	0.8340	0.2064	13.7045
2	0.9468	0.9257	-0.1766	0.7521	0.2883	10.8044
3	0.6915	1.0138	-0.2276	0.6235	0.4169	7.5995
4	0.4395	1.0514	-0.2659	0.4847	0.5556	5.1040
5	1.2014	0.9351	0.0248	0.9701	0.0703	23.0631
6	0.7733	0.8349	-0.2616	0.5956	0.4448	7.0373
7	0.1860	0.9494	0.1394	0.4683	0.5721	4.8505
8	0.3392	0.9918	-0.2265	0.4257	0.6147	4.2268
9	0.8194	0.8489	-0.0677	0.6993	0.3411	9.3420
10	0.2361	0.8252	0.1695	0.4658	0.5746	4.8130
11	0.5843	0.8039	-0.3202	0.4606	0.5798	4.7338
12	0.4016	0.8907	-0.2817	0.4050	0.6354	3.9390
13	0.6082	0.7870	0.0008	0.5904	0.4500	6.9364
14	0.6631	0.8165	-0.1011	0.5911	0.4493	6.9491
15	0.5945	0.7802	-0.2358	0.4905	0.5499	5.1937
16	0.5361	0.7170	-0.3813	0.3823	0.6581	3.6347

Table 9. Average S/N ratio of CQL.

Symbol	Machining parameters	Average S/N ratio				Optimal result	Delta	Rank
		Level-1	Level-2	Level-3	Level-4			
<i>d</i>	Depth of cut	9.303	9.794	5.707	5.678	2	4.116	3
<i>f</i>	feed	13.261	7.401	5.594	4.226	1	9.035	1
<i>v</i>	Cutting speed	7.278	10.75	7.029	5.426	2	5.324	2

Table 10. ANOVA for S/N ratio of CQL.

Parameters	DF	SS	MS	F	P	% contribution	Remarks
<i>d</i>	3	59.961	19.987	2.12	0.199	16.34	Insignificant
<i>f</i>	3	189.984	63.328	6.71	0.024	51.77	Significant
<i>v</i>	3	60.308	20.103	2.13	0.198	16.43	Insignificant
Error	6	56.663	09.444				
Total	15	366.916					

Table 11. Consequences of confirmation trial for multi-responses.

	Initial setting	Optimal setting $d2-f1-v2$	
	$d1-f1-v1$	Prediction	Experiment
VBc (mm)	0.077		0.089
Ra ( $\mu\text{m}$ )	0.552		0.438
CRC	1.867		1.766
CQL	0.2064		0.0703
S/N Ratio of CQL (dB)	13.7045	18.5635	23.0631
Gain in S/N ratio of CQL = 9.3586			

### CONCLUSION

A research was performed for optimisation of JIS S45C steel hard turning process parameters with multiple performance characteristics on the basis of an orthogonal array (OA) with WPCA coupled with Taguchi approach. The analysis presented is an integrated approach of regression, BNN, RNN and WPCA method for the modelling and optimisation of technological factors to attain lower surface roughness, cutting tool-wear and chip reduction coefficient in hardened steel application. The summaries of the analysis can be presented as follows:

- i. Higher micro-hardness confirms the higher wear resistance capability of cutting insert and it confirms from the experimental wear result data where up to 140 m/min turning speed the maximum wear width is 0.176 mm which far lower than the criteria cap of flank wear 0.3 mm. Turning with 240 m/min of cutting speed is not recommended to machine the hardened steel with a higher depth of cut condition.
- ii. Abrasion and built up-edge are the more dominant mode of tool-wear at low and moderate cutting speed while the catastrophic failure of tool-tip is identified at higher cutting speed condition.
- iii. Turning at higher cutting feed (0.35 mm/rev) is not suitable to get the good quality of finish. Up to 0.25 mm/rev of feed is recommended to get less than 1.6  $\mu\text{m}$  surface roughness. Feed rate was identified as the most influencing term for surface roughness as the gap between two consecutive marks on finished surface increases with feed value.
- iv. Broken discontinuous types chips are produced at higher feed rate and highest depth of cut condition which attributes the poor quality of finish and not favourable for hard turning concern.
- v. Higher CRC values are noticed at higher depth of cut (0.5 mm) conditions i.e. may be higher cutting forces thus higher power required to machine the hardened steel. Also, higher mean  $R_a$  value is noticed from experimental result data which confirms the higher cutting forces generation during machining. However, the depth of cut 0.5 mm is not suitable for the present work.
- vi. All three modelling techniques (Regression, BNN, and RNN) are suitable to predict the responses. The maximum mean absolute for  $VB_c$ ,  $R_a$ , and CRC is found as 5.05% (regression modelling), 4.56% (RNN with 3-8-1 structure) and 2.47% (regression). BNN with 3-8-1 network architecture model is more suitable to predict the responses compared to other models.

- vii. From WPCA, the optimal data set is found as  $d_2$  (0.3 mm) –  $f_1$  (0.05 mm/rev) –  $v_2$  (120 m/min) and from confirmatory trial the  $VB_c$  is 0.089 mm,  $R_a$  is 0.438  $\mu$ m and CRC is 1.766 observed and at the optimal condition, CQL value is increased by 9.3586 (i.e. 68.3%) from the initial process parameter setting that provides a better use of WPCA approach in machining.

A systematic methodology was presented to design and investigation of the experimental scheme, which is able to minimise the surface roughness, flank wear, and chip reduction coefficient that is valuable to other researchers and machinist and eye-opening for further research on surface finish, wear and chip morphology. Further study may consider the various chip breaker pattern and its geometry on the rake face of the tool in hard machining. Furthermore, the hard machining can be investigated by varying the work hardness, tool geometry, grade of coated carbide inserts and cutting environment. Also, the aspects of microstructure, surface integrity, cutting force, tool conditioning monitoring can be considered as future work.

### **ACKNOWLEDGEMENT**

Authors express their gratitude's to Dyna Force Hydraulics Pvt. Ltd., Pune, India for supplying the test specimen and also thankful to KIIT Deemed to be University, Bhubaneswar for providing the experimental facilities.

### **REFERENCES**

- [1] Adamik M, Drlicka R, Matus M, Zitnansky J. Effectiveness of hard turning. *Advanced materials research*. Trans Tech Publications 2013; 801: 109-116.
- [2] Tamizharasan T, Selvaraj T, Haq AN. Analysis of tool wear and surface finish in hard turning. *The International Journal of Advanced Manufacturing Technology* 2006; 28(7-8): 671-679.
- [3] Guddat J, M'Saoubi R, Alm P, Meyer D. Hard turning of AISI 52100 using PCBN wiper geometry inserts and the resulting surface integrity. *Procedia Engineering* 2011; 19: 118-124.
- [4] Panda A, Das SR, Dhupal D. surface roughness analysis for economic feasibility study of coated ceramic tool in hard turning operation. *Process Integration and Optimisation for Sustainability* 2011; 1(4): 237-249.
- [5] Tonshoff HK, Arendt C, Amo R Ben. Cutting of hardened steels. *Annals of the CIRP* 2000; 49/2: 547–566.
- [6] Liew PJ, Shaaroni A, Sidik NAC, Yan J. An overview of current status of cutting fluids and cooling techniques of turning hard steel. *International Journal of Heat and Mass Transfer* 2017; 114: 380–394.
- [7] Chinchankar S, Choudhary SK, Machining of hardened steel-experimental investigations, performance modelling and cooling technique: A review. *International Journal Machine Tools and Manufacturing* 2015; 89: 95-109.
- [8] Sampaio MA, Machado AR, Laurindo CAH, Torres RD, Amorim FL. Influence of minimum quantity of lubrication (MQL) when turning hardened SAE 1045 steel: A comparison with dry machining. *International Journal of Advanced Manufacturing Technology* 2018; 98(1-4): 959-968.
- [9] Singh T, Dureja JS, Dogra M, Bhatti MS. Machining performance investigation of AISI 304 austenitic stainless steel under different turning environments. *International Journal of Automotive and Mechanical Engineering* 2018; 15(4): 5837-5862.

- [10] Kumar R, Sahoo AK, Mishra PC, Das RK. Comparative investigation towards machinability improvement in hard turning using coated and uncoated carbide inserts: Part I experimental investigation. *Advances in Manufacturing* 2018; 6(1): 52-70.
- [11] Hadi H, Tajul L, Zailani ZA, Hussin MS. The parametric effect and optimisation on JIS S45C steel turning. *International Journal of Engineering Science and Technology* 2011; 3(5): 4479-4487.
- [12] Yap TC, Lim CS, Leau JW. Surface roughness and cutting forces in cryogenic turning of carbon steel. *International Journal of Engineering Science and Technology* 2011; 7(10): 911-920.
- [13] Tanaka R, Yamane Y, Sekiya K, Narutaki N, Shiraga T. Machinability of BN free-machining steel in turning. *International Journal of Machine Tools and Manufacture* 2007; 47: 1971–1977.
- [14] Chau NL, Nguyen MQ, Dao TP, Huang SC, Hsiao TC, Cong DD, Dang VA. An effective approach of adaptive neuro-fuzzy inference system-integrated teaching learning-based optimisation for use in machining Optimisation of S45C CNC turning. *Optimisation and Engineering* 2018 <https://doi.org/10.1007/s11081-018-09418-x>.
- [15] Tiwari R, Das DK, Sahoo AK, Kumar R, Das RK, Routara BC. Experimental investigation on surface roughness and tool wear in hard turning JIS S45C steel. *Materials Today: Proceedings* 2018; 5: 24535–24540.
- [16] Erkan Ö, Işık B, Çiçek, A, Kara F. Prediction of damage factor in end milling of glass fibre reinforced plastic composites using artificial neural network. *Applied Composite Materials* (2013); 20(4): 517-536.
- [17] Mia M, Dhar NR. Modelling of surface roughness using RSM, FL and SA in dry hard turning. *Arabian Journal of Science and Engineering* 2018; 43(3): 1125-1126.
- [18] Meddour I, Yallese MA, Bensouilah H, Khellaf A, Elbah M. Prediction of surface roughness and cutting forces using RSM, ANN and NSGA-II in finish turning of AISI 4140 hardened steel with mixed ceramic tool. *The International Journal of Advanced Manufacturing Technology* 2018; 97(5-8): 1931–1949.
- [19] Labidi A, Tebassi H, Belhadi S, Khettabi R, Yallese MA. Cutting conditions modelling and optimisation in hard turning using RSM, ANN and desirability function. *Journal of Failure Analysis and Prevention* 2018; 18(4): 1017-1033.
- [20] Das A, Mukhopadhyay A, Patel SK, Biswal BB. Comparative assessment of machinability aspects of AISI 4340 alloy steel using uncoated carbide and coated cermet inserts during hard turning. *Arabian Journal of Science Engineering* 2016; 41(11): 4531-4552.
- [21] Kumar R, Sahoo AK, Das RK, Panda A, Mishra PC. Modelling of flank wear, surface roughness and cutting temperature in sustainable hard turning of AISI D2 steel. *Procedia Manufacturing* 2018; 20: 406–413.
- [22] Paturi UMR, Devarasetti H, Narala SKR. Application of regression and artificial neural network analysis in modelling of surface roughness in hard turning of AISI 52100 Steel. *Materials Today: Proceedings* 2018; 5(2): 4766-4777.
- [23] Yıldırım CV, Kıvak T, Erzincanlı F. Tool wear and surface roughness analysis in milling with ceramic tools of Waspaloy: a comparison of machining performance with different cooling methods. *Journal of the Brazilian Society of Mechanical Sciences and Engineering* (2019); 41(2), 83.
- [24] Panda A, Das SR, Dhupal D. Hard turning of HSLA steel with coated ceramic inserts: An assessment, modelling, optimisation and cost analysis. *International Journal of Automotive and Mechanical Engineering* 2018; 15(4): 5890-5913.
- [25] Kumar R, Sahoo AK, Mishra PC, Das RK. Comparative investigation towards machinability improvement in hard turning using coated and uncoated carbide inserts: Part II 7339modelling, multi-response Optimisation, tool life, and economic aspects. *Advances in Manufacturing* 2018; 6(2): 155-175.

- [26] Kumar R, Sahoo AK, Mishra PC, Das RK. Measurement and machinability study under environmentally conscious spray impingement cooling assisted machining. *Measurement* 2019; 135: 913-927.
- [27] Kumar R, Sahoo AK, Mishra PC, Das RK. An investigation to study the wear characteristics and comparative performance of cutting inserts during hard turning. *International Journal Machining and Machinability of Materials* 2018; 20(4): 320-344.
- [28] Bhushan B, *Modern tribology handbook*, CRC press, 1<sup>st</sup> Edition 2000.
- [29] Kumar R, Sahoo AK, Mishra PC, Das RK. Performance of near dry hard machining through pressurised air water mixture spray impingement cooling environment. *International Journal of Automotive and Mechanical Engineering* 2019;16(1): 6108-6133.
- [30] Ueda N, Matsuo T, Uehara K. An analysis of saw-toothed chip formation. *CIRP Annals*. 1982; 31(1): 81-84.
- [31] Murugappan SH, Arul S. Effect of Cryogenic Pre cooling on chip reduction co-efficient during turning of EN8 steel rod 2017; 4(8): 8848-8855.
- [32] Senthilkumar N, Tamizharasan T. Effect of tool geometry in turning AISI 1045 steel: Experimental investigation and FEM analysis. *Arabian Journal of Science and Engineering* 2014; 39(6): 4963-4975.
- [33] Das A, Patel SK, Hotta TK, Biswal BB. Statistical analysis of different machining characteristics of EN-24 alloy steel during dry hard turning with multilayer coated cermet inserts. *Measurement* 2019; 134:123–141.
- [34] Mia M, Dhar NR. Prediction of surface roughness in hard turning under high pressure coolant using artificial neural network. *Measurement* 2016; 92: 464–474.
- [35] Zhang GG, Patuwo BE, Hu MY. Forecasting with artificial neural networks: The state of the art, *International Journal of Forecasting* 1998; 14 (1): 35–62.
- [36] Panchal FS, Panchal M. Review on methods of selecting number of hidden nodes in artificial neural network. *International Journal of Computer Science and Mobile Computing* 2014; 3(11): 455-464.
- [37] Muller AT, Hiss JA, Schneider G. Recurrent neural network model for constructive peptide design. *Journal of Chemical Information and Modelling* 2018; 58(2): 472-479.
- [38] Medskar LR, Jain LC. *Recurrent neural networks design and applications*. CRC Press LLC. 2001.
- [39] Pham DT, Karaboga D. Training Elman and Jordan networks for system identification using genetic algorithms. *Artificial Intelligence in Engineering* 1999; 13(2):107-117.
- [40] Mello GD, Pai PS, Puneet NP. Optimisation studies in high speed turning of Ti-6Al-4V. *Applied Soft Computing* 2017; 51:105–115.
- [41] Kumar R, Das RK, Sahoo AK, Mishra PC, Roy S. ANN modelling of cutting performances in spray cooling assisted hard turning. *Materials Today: Proceedings* 2018; 5: 18482–18488.
- [42] Wang W, Lu Y. Analysis of the mean absolute error (MAE) and the root mean square error (RMSE) in assessing rounding model. *IOP Conference Series: Material Science and Engineering* 324 012049.
- [43] Routara BC, Mohanty SD, Datta S, Bandyopadhyay A, Mahapatra SS. Combined quality loss (CQL) concept in WPCA-based Taguchi philosophy for Optimisation of multiple surface quality characteristics of UNS C34000 brass in cylindrical grinding. *The International Journal of Advanced Manufacturing Technology* 2010; 51(1): 135-143.
- [44] Das D, Mishra P, Singh S, Chaubey A, Routara B. Machining performance of aluminium matrix composite and use of WPCA based Taguchi technique for multiple response optimisation. *International Journal of Industrial Engineering Computations* 2018; 9(4): 551-564.
- [45] Tong LI, Wang CH, Chen CH. Optimisation of multiple responses using principal component analysis and technique for order preference by similarity to ideal solution, *International Journal of Advanced Manufacturing Technology* 2005; 27(3):407-414.